scientific reports

Check for updates

OPEN

Gamma-radiation insulating performance of AlON-hardened $Na_2O–Bi_2O_3–SiO_2–BaO–Fe_2O_3–ZrO_2$ glasses

Jamila S. Alzahrani[1]✉, Z. A. Alrowaili[2], I. O. Olarinoye[3], Chahkrit Sriwunkum[4], Imen Kebaili[5] & M. S. Al-Buriahi[6]

Aside high radiation cross-section, high mechanical strength is an essential quality for durable and effective glass shields. Many emerging glass shields are brittle with low strength parameters; consequently, limiting their longstanding applications. In this study, the use of AlON (aluminium oxynitride) to increase the hardness of a Zr-based glass system and the consequent effects on the glass density and gamma shielding capacity were investigated. AlON was produced from a combination of AlN and Al_2O_3 powders through the solid-phase reaction process at 1750 °C. The melt-and-quench process was then used to make the Zr-based ($Na_2O–Bi_2O_3–SiO_2–BaO–Fe_2O_3–ZrO_2$) glass. The glass was homogeneously mixed with varying quantities (0 (GZr8), 4 (GZr8Al4), and 8% (GZr8Al8) by weight) of AlON powder. Using the FLUKA Monte Carlo code, the gamma photon interaction parameters of the AlON-doped glasses were obtained. The density of the glasses increased from 2.90 to 3.11 g/cm^3 as the AlON mass proportion increased from 0 to 8%. For GZr8, GZr8Al4, and GZr8Al8, the mass attenuation coefficient had values in the range 0.0316–38.9421 cm^2/g, 0.0315–38.8504 cm^2/g, and 0.0311–37.0391 cm^2/g, respectively. The range of the half-value layer and mean free path for 0.015–15 MeV photons is about 0.01–7.54 cm and 0.01–10.87 cm for GZr8, 0.01–7.19 cm and 0.01–10.38 cm for GZr8Al4, and 0.01–7.14 cm and 0.01–10.31 cm for GZr8Al8. The introduction of AlON into the glass matrix quenched photon buildup factors and enhanced the photon shielding ability of the GZr8 glass system. GZr8Al8 can displace many existing shielding materials, including glasses, concrete, and rocks, based on the analysis of the obtained results. Aside high gamma shielding efficiency, the mechanical strength and Pb-free nature are other attractive features that give the AlON-doped glasses an edge over many existing gamma shielding materials. The present glass system is useful for durable gamma-ray shielding of small-scale gamma sources gamma sources applied in medicine and radiation research.

Keywords Dose-rate, Gamma-radiation, Glass-ceramics, Monte-Carlo-simulation, Radiation protection

The quantification of gamma-ray transmission level and energy deposition processes are essential in many technical and research fields. Traditionally, gamma radiation is an essential tool in the health sector for probing the health status of humans and animals, treating diseases, and sterilizing equipment[1–3]. Gamma radiation is also used for airport security, testing the quality of manufactured materials, food production and preservation, crop and micro-organism culturing and growth control, material characterization and property control[4–10]. Gamma radiation is a product of natural and technologically induced nuclear processes, therefore, it is ubiquitous in the Earth surface and environment. Based on the successes recorded in the existing applications and the availability of measures to prevent nuclear radiation accident, the scope of radiation applications can be projected to expand. Accidental exposure of gamma radiation can result in undesirable effects such as, cell mutation, disease, death, and damages to materials and gadgets, hence, the control of ionizing radiation is essential.

[1]Department of Physics, College of Science, Princess Nourah bint Abdulrahman University, P.O. Box 84428, 11671 Riyadh, Saudi Arabia. [2]Department of Physics, College of Science, Jouf University, P.O.Box 2014, Sakaka, Saudi Arabia. [3]Department of Physics, School of Physical Sciences, Federal University of Technology, Minna, Nigeria. [4]Department of Physics, Ubon Ratchathani University, Ubon Ratchathani, Thailand. [5]Department of Physics, Faculty of Science, King Khalid University, P.O. Box 9004, Abha, Saudi Arabia. [6]Department of Physics, Sakarya University, Sakarya, Turkey. ✉email: alburiahi@sakarya.edu.tr

To mitigate the unwanted effects of uncontrolled exposure in human environments, radiation protection measures, including the use of shields have been emphasized and enforced and advised by local authorities and international organizations, respectively, in many areas where radiation are deployed for the benefits of mankind and the biota. Many materials have the potential to function as shields in radiation environments, however, different radiation application areas (such as the aerospace, health, research, manufacturing, agricultural, food and nuclear industries), require distinct qualities for effective shielding performance. In the past, Pb and Pb-based materials were preferred for gamma and x-ray shielding, because of the high photon cross-section that Pb exhibits. However, the fear of poisoning and its high density has made the use of Pb unpopular in many conventional radiation applications and in scenarios where light shields are preferred. Concrete blended from different aggregates is popular for biological shields, its opaqueness and instability also restrict its application in high temperature and extreme environments, security observatories and the airspace industries for shielding. The use of rocks and metals are also limited by their opaque nature. The limitations imposed by the inherent properties of potential shielding materials prevent their applications as radiation insulators in certain radiation environments. In addition, the unique requirements imposed by radiation environments also make it hard to have a universal shield for all radiation environments. Therefore, recent investigations[11–26] have focused on finding novel materials with superior shielding and dosimetry competences and having attractive properties that delineate the environments where they are most suitable or stable, and functional as radiation protective barriers. In addition, the economics of producing novel materials from pristine raw materials have made researchers to investigate the open-loop recycling of waste materials for shielding applications[20–26].

In recent times, depending on their chemical configurations, glasses have been recognized as effective and sometimes durable shields compared to traditional shields such as lead (Pb), metals and their alloys, and concrete. This is a result of some of the attributes of glasses which have attracted radiation-protection scientist and technicians. These features include, flexibility in the choice of chemical configuration, ease and low cost of production. These properties make it easy to tailor glsass properties, produce cheap, durable and effective glass shields that fits into different radiation environments. Consequently, many glass matrices have been produced and characterized for their radiation shielding parameters and other characteristics that define where they can be deployed for radiation control applications, especially in recent times[27–33]. Also, these previous studies have highlighted the roles of different chemical admixtures in projecting diverse aspects of the properties and functionalities of glass systems. For instance, glasses that are optically active and having high radiation absorption cross-sections are preferred as transparent shields, radiation detectors and dosimeters[20–31]. Also, chemically unreactive and thermally resilient glasses are preferred in harsh nuclear environments, such as space and nuclear reactors. Durable and tough glasses are also attractive for nuclear waste management and radiation control. Clearly, the thermal response, optical behavior, strength, and chemical durability of glasses are some of the factors that determine where glasses with high gamma absorption features can be used for shielding.

Glasses are generally brittle; this limits their mechanical strength and functionality. Therefore, in modern glass manufacturing, mechanical performance is a key issue of interest[34]. Recently, the improvement of mechanical strength, brough about by playing around the chemistry of materials, synthesis method, and post-production treatment, or a combination of the three, has allowed for a wide range of glass applications over the past 10 years. For instance, there has been tremendous improvement in damage resistance of covering glasses of handheld devices in recent times[34–36]. This has improved the durability and market value of the gadgets. Despite this progress, the limitations of glass brittleness and low hardness continue to constrain some glass matrices in many applications. Moreover, deliberately increasing the mechanical strength and hardness of glasses intended for radiation shields is scarce in the literature.

In this study, the use of AlON (aluminium oxynitride) to increase the hardness of a Zr-based glass system ($Na_2O–Bi_2O_3–SiO_2–BaO–Fe_2O_3–ZrO_2$) and the consequent effects on the glass density and gamma shielding capacity is investigated. The glass composition is interesting and chosen to give a balance between low and high atomic number modifying oxides. The inclusion of Bi_2O_3, ZrO_2, and BaO serves to stabilize the glass structure and increase the gamma-cross-section due to their density and affective atomic number[37,38]. On the other hand, Na_2O is a good network stabilizer which can also help to improve the mechanical strength of glasses[37]. Also, AlON is known to possess high hardness, strength, and resistant to abrasion[39]. This study attempts to improve the mechanical aspect of the glass system without degrading its gamma radiation absorption prowess. This research produced mechanically strong and durable Zr-based glasses with good gamma radiation insulating properties for practical applications gamma-shields in medical and other radiation-based facilities. It also highlights the use of AlON as n hardening agent for shielding glasses. This study is important from material chemistry and development perspectives and useful for radiation protection of man and the environment.

Materials and method

Aluminum nitride (AlN) and Al_2O_3 (alumina) powders of 35.7 mol% and 64.3 mol% concentration, respectively were blended together and reacted through the solid-phase reaction process at 1750 °C to produce AlON. The obtained powder was compressed into pellets using a steel die. Then, using the cold isostatic pressing method, the pellets were densified further. The resulting pellets were sintered for 4 h at 1750 °C in a N_2 environment. The high temperature reactive sintering is required to achieve homogenous and completely dense samples[40]. The AlON powder compacts were then ground into a powder using a vibrating disc mill.

The melt-and-quench was used to make the Zr-based ($Na_2O–Bi_2O_3–SiO_2–BaO–Fe_2O_3–ZrO_2$) glass. All the chemical reagents were purchased from Merck. For 20 min, the components that made up the glass composition were melted at 1350 °C. The uniform material was placed into a mold to cool after melting. The bulk glass was heated to 250 °C for 8 h in order to anneal it. Grinded in an agate mortar, the glass was powdered to serve as a matrix for AlON doping. Ultimately, the glass was homogeneously mixed with AlON powder in varying quantities (0, 4, and 8% by weight) and pressed in the die to create an AlON-reinforced Zr-based glass–ceramic composite. To increase their density, sample composites underwent cold isostatic pressing. For ninety minutes, the resulting samples were sintered at 570 °C. The sample code and chemical makeup of the prepared sample, as determined by the X-ray fluorescence analysis are displayed in Table 1.

The glass–ceramics samples' physical, mechanical, and radiation response qualities were ascertained by a variety of experimental and theoretical methods. The popular Archimedes method was used to determine the densities of the samples. The mass of the glass–ceramics in air (M_{air}) and when complete immersed in xylene (M_{xylene}) was taken. Using the density of xylene (0.863 g/cm^3), the densities of the produced glass–ceramics were determined as:

$$\rho\left(\frac{g}{\mathrm{cm}^3}\right) = \frac{M_{air} \times 0.863}{M_{air} - M_{xylene}} \quad (1)$$

In addition, the effect of adding AlON on the mechanical hardness of the Zr-based glasses was determined using the micro-indentation hardness test. The test was performed by the Vickers hardness instrument using a force of 20 N for 15 s.

In conclusion, the gamma photon interaction parameters of the synthesised samples were obtained for gamma-ray energies (E) within 15 keV ≤ E ≤ 15 MeV using FLUKA simulations and computation methods. First, the mass attenuation coefficients (μ/ρ) of the glass ceramics were obtained using photon transmission simulations in the FLUKA Monte Carlo code environment. Figure 1 summarises the simulation arrangement in the FLUKA program. To ascertain the acceptability of the simulation arrangement, accuracy of the transmission data, and μ/ρ obtained therein, the values of μ/ρ of the samples were also computed using XCOM[41] for the same energy spectrum as FLUKA simulations. FLUKA is a Monte Carlo code which can be used to perform the simulation of the interaction and transmission processes of radiation of different qualities. For gamma photon transmission simulation, the input file specifies the beam source, number of incident photons, energy, and position. Also, among the interacting material, its dimension, and geometry of the setup is described in the input file. The entire setup is surrounded by a black hole environment where all radiation is absorbed due to infinite radiation absorption cross-section. FLUKA has a friendly user interface called flair where input files are created and edited and the output files can be viewed. A card is used to define keywords and argument. The BEAM, BEAMPOS, Geometry, and Media cards were used to define the beam characteristics, position and direction of the primary beam, geometry of the setup, and define the interactive medium, respectively, while the scoring card was used to record the transmitted particles. More details of local deployment can be found in previous articles[42–44]. Other photon interaction parameters were computed either using the NIST database[41] or direct computation from the values of the μ/ρ based on standard computation procedures as previously highlighted[45–48]. The computed parameters include: linear attenuation coefficient (μ), half-value layer (HVL), mean free path (λ), effective electron density (N_{eff}), effective atomic number (Z_{eff}), specific gamma constant (Γ), mass energy absorption coefficient $\frac{\mu_{en}}{\rho}$, dose rates (D_r) at different sample thicknesses. Expressions for evaluating these quantities can be found in[11–26]. The exposure (EBF) and energy absorption (EABF) buildup factors were computed based on the geometric progression fitting process[30,49].

Results and discussion

In Table 1, the measured density and Vickers hardness values of the prepared glasses (GZr8, GZr8Al4, and GZr8Al8) are presented. Both parameters increase with the AlON content of the glasses. While density increases from 2.90 to 3.11 ± 0.01 g/cm^3, hardness increases from 4.89 to 6.33 GPa as the AlON mass proportion increases from 0 to 8%. The observed growth in the value of density could be attributed to the increase in the weight concentrations of dense metals (such as Ba and Bi) in the glasses, when AlON was introduced. This increases the weight per unit volume and the glass system become more compact. The values of the hardness reveal that AlON increases the resilience of the glasses against mechanical failure and deformation. This shows that adding AlON

	Glass sample		
Composition (wt%)	**GZr8**	**GZr8Al4**	**GZr8Al8**
N	0.00000	0.24341	0.54138
O	35.30582	36.38945	36.51223
Na	7.70761	6.80527	6.95471
Al	0.00000	1.79513	3.58147
Si	12.68026	11.60243	11.30661
Fe	1.47190	1.40974	0.93701
Zr	11.34759	10.04057	9.78657
Ba	6.27548	6.29817	6.44456
Bi	25.21134	25.41582	23.93545
Density (g/cm^3)	2.90	3.05	3.11
Vickers Hardness (GPa)	4.89	5.94	6.33

Table 1. Sample code and weight fraction (wt.%) of compound present in the prepared glasses including their measured density and hardness.

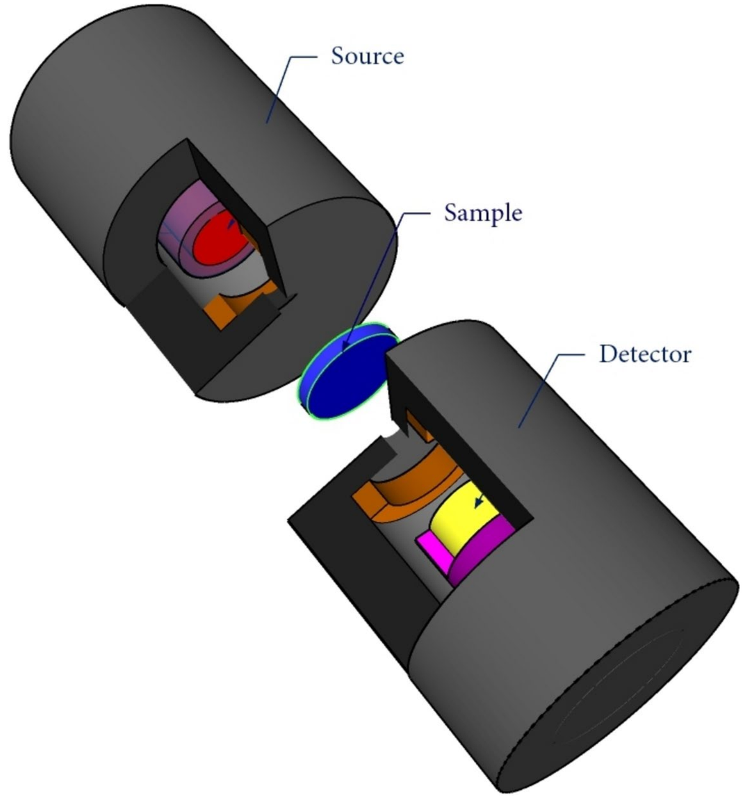

Fig. 1. FLUKA simulation setup used for evaluating the gamma-ray transmission parameters of the prepared glasses.

could enhance the toughness, compactness, and mechanical attributes of a glass matrix. This abrasive resistance nature of the AlON-rich glasses makes them useful for high strength applications such as in construction industry or nuclear waste management.

The values of μ/ρ obtained from FLUKA simulations and XCOM software and the absolute differences between both set of values are tabulated for each glass material and energy in Table 2. The values of μ/ρ computed from FLUKA Monte Carlo simulation data and direct computation using XCOM have good direct correlation, as the variations between them were less than 1%. The implication of this is that the adopted simulation geometry approximates a narrow beam photon transmission setup. The insignificant differences in the values could be attributed to error associated with counting statistics in FLUKA and slight differences in the cross-section data library in XCOM and FLUKA. Due to the insignificant differences in the obtained μ/ρ from both methods, the simulation technique could therefore be used to investigate photon interaction processes and obtain interaction parameters for other materials.

Using the FLUKA-simulation-generated μ/ρ values in Table 2, it is clear that the mass attenuation coefficients of the glasses vary with gamma-ray energy (E), and AlON content. Figure 2 shows the changes in the values of μ/ρ with respect to E for μ/ρ and μ. Due to the direct mathematical relationship between μ and μ/ρ (Eq. 2), the plots of both attenuation coefficients vary in similar ways with photon energy, E.

$$\mu = \rho * {}^{\mu}/_{\rho} \tag{2}$$

The attenuation coefficients decrease with E for 15 keV ≤ E ≤ 8 MeV, but slightly increase afterwards. For GZr8, GZr8Al4, and GZr8Al8, μ/ρ had the highest values for GZr8 sample. The changes in the attenuation coefficients can be described by dividing the energy spectrum into three unique regions. Firstly, for E ≤ 60 keV, there was a rapid decay in attenuation coefficients. Second, for 60 ≤ E ≤ 8 MeV, the decay continued but at a slower pace, except at 100 keV, where a bump was observed. Lastly, the high energy region (E > 8 MeV), the values of the attenuation coefficients increase gradually. To explain these, it is important to consider how the gamma-photon interaction cross-sections for photoelectron creation (PEC), Compton scattering (CS), and pair creation (PC) behave as functions of energy. Hence,

$$\frac{\mu}{\rho} \cong (\mu/\rho)_{PEC} + (\mu/\rho)_{CS} + (\mu/\rho)_{PC} \tag{3}$$

where $(\mu/\rho)_i$ refers the process interaction of PEC, CS, and PC to the μ/ρ. For photons energy E, incident on an atom with Z, $(\mu/\rho)_i$ [50,51]:

	GZr8			GZr8Al4			GZr8Al8		
Energy (MeV)	XCOM	FLUKA	Dev.%	XCOM	FLUKA	Dev.%	XCOM	FLUKA	Dev.%
0.015	39.17242	38.94213	0.588	39.07858	38.85041	0.584	37.24691	37.03906	0.558
0.02	34.03242	33.94164	0.267	33.26612	33.20525	0.183	31.73301	31.67963	0.168
0.03	11.87849	11.87552	0.025	11.61840	11.62273	0.037	11.08293	11.08575	0.025
0.04	6.86797	6.85213	0.231	6.75545	6.74667	0.130	6.53367	6.52533	0.128
0.05	3.85943	3.84530	0.366	3.79992	3.78900	0.287	3.67769	3.66729	0.283
0.06	2.42138	2.40538	0.661	2.38633	2.37493	0.478	2.31125	2.30054	0.464
0.08	1.18988	1.17804	0.995	1.17489	1.16490	0.850	1.14008	1.13088	0.807
0.1	1.78958	1.78326	0.353	1.79066	1.78396	0.374	1.70812	1.70195	0.361
0.15	0.69672	0.69424	0.356	0.69759	0.69517	0.347	0.66882	0.66659	0.334
0.2	0.38251	0.38220	0.082	0.38308	0.38327	0.048	0.36963	0.36981	0.050
0.3	0.19284	0.19230	0.280	0.19314	0.19306	0.044	0.18854	0.18845	0.051
0.4	0.13421	0.13334	0.649	0.13441	0.13421	0.154	0.13227	0.13212	0.107
0.5	0.10744	0.10691	0.496	0.10759	0.10744	0.136	0.10641	0.10634	0.064
0.6	0.09210	0.09158	0.564	0.09222	0.09179	0.461	0.09150	0.09108	0.456
0.8	0.07469	0.07444	0.334	0.07478	0.07465	0.181	0.07447	0.07433	0.195
1.0	0.06457	0.06408	0.759	0.06464	0.06419	0.709	0.06450	0.06406	0.685
1.5	0.05097	0.05053	0.862	0.05102	0.05058	0.860	0.05099	0.05056	0.836
2	0.04436	0.04403	0.747	0.04440	0.04408	0.726	0.04435	0.04403	0.720
3	0.03782	0.03745	0.986	0.03782	0.03746	0.968	0.03771	0.03734	0.966
4	0.03475	0.03443	0.923	0.03472	0.03439	0.936	0.03453	0.03421	0.938
5	0.03314	0.03288	0.789	0.03309	0.03281	0.841	0.03284	0.03256	0.844
6	0.03229	0.03209	0.612	0.03221	0.03201	0.621	0.03191	0.03171	0.626
8	0.03171	0.03159	0.370	0.03160	0.03148	0.378	0.03121	0.03109	0.394
10	0.03186	0.03176	0.320	0.03172	0.03161	0.324	0.03126	0.03115	0.341
15	0.03322	0.03314	0.232	0.03302	0.03293	0.289	0.03243	0.03251	0.255

Table 2. Mass attenuation coefficient of the prepared glasses via FLUKA and XCOM at different photon energies.

$$\left(\frac{\mu}{\rho}\right)_{PEC} \propto Z^5 / E^{3.5} \tag{4}$$

$$\left(\frac{\mu}{\rho}\right)_{CS} \propto Z^2 / E \tag{5}$$

$$\left(\frac{\mu}{\rho}\right)_{PC} \propto Z^2 \ln\left(E - 2m_e\right) \tag{6}$$

Equations 4, 5 and 6 shows that the PEC process accounts for the high but rapidly decreasing values of μ/ρ in the first energy division while the CS and PC processes dictates the trend of μ/ρ in the two latter energy divisions, respectively. The sudden rise in the attenuation coefficients at 100 keV is attributed to the K-absorption edge of Bi atoms. Due to high photoelectric absorption of photons at absorption edges, μ/ρ spectra often show high values at absorption edges of atoms.

Comparatively, the μ/ρ at each energy follows the order: $(\mu/\rho)_{GZr8} < (\mu/\rho)_{GZr8Al4} < (\mu/\rho)_{GZr8Al8}$ for most of the energy spectrum. The order is reversed at 15 keV due to the proximity of the energy to absorption edges of low atomic number atoms which have higher concentrations in the AlON-deficient samples. However, the former order is consistent with the density and AlON content of the glasses. The introduction AlON increases the weight proportions of Ba, and Bi, two atoms with high $(\mu/\rho)_i$. This ultimately increased the effective Z of the glass system, hence, the observed growth in the value of μ/ρ. AlON thus increased the gamma-interaction probabilities of the glass system.

The description of the shielding capacity of a medium is often conveniently stated in terms of linear thicknesses. Two parameters are often used for this purpose: the mean free path (λ) and the half-value layer ($d_{1/2}$). These parameters can be evaluated directly from the values of μ/ρ according to the following equations[52–56]:

$$\lambda = \frac{1}{\rho \times \mu/\rho} \tag{7}$$

$$d_{1/2} = \frac{\ln 2}{\rho \times \mu/\rho} \tag{8}$$

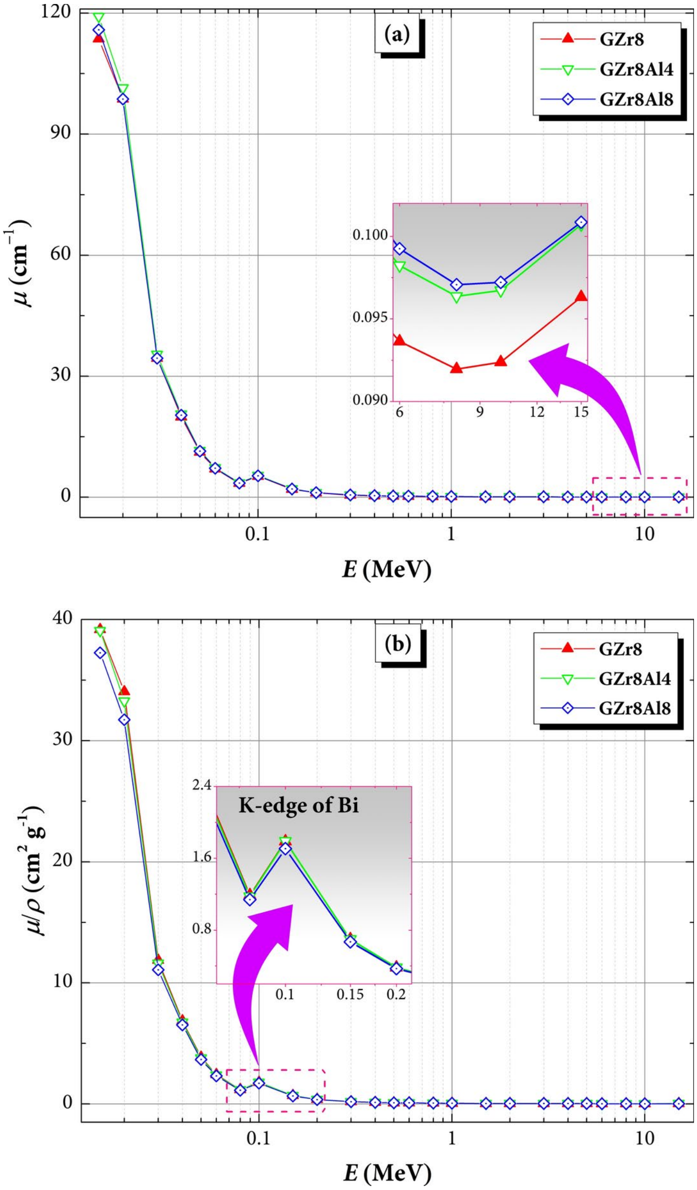

Fig. 2. (**a**) Linear attenuation coefficient (μ) and (**b**) mass attenuation coefficient (μ/ρ) of the prepared glasses with different photon energies.

The former is a measure of the distance moved between interactions by photons, while the latter gives the thickness required to attenuate incident photon beams by 50%. The two quantities vary inversely as the attenuation coefficients; hence, lower λ and $d_{1/2}$ are indications of e better attenuation prowess and thinner absorber is required to achieve a specific radiation transmission level. In Fig. 3, the spectra of $d_{1/2}$ and λ are shown for the investigated glasses. The E-variations of the two parameters are approximately the inverses of the attenuation coefficient and the order of $d_{1/2}$ at each energy is $\left(d_{1/2}\right)_{GZr8} > \left(d_{1/2}\right)_{GZr8Al4} > \left(d_{1/2}\right)_{GZr8Al8}$. The trend is the same for λ. $d_{1/2}$ One can say that the thickness of AlON-rich glasses required for photon absorption is lower. It can be concluded that the addition of AlON to the glass matrix lowers the distance travelled by photons between interactions and makes the glasses less transparent to gamma radiation. Furthermore, the spectra show that the thickness of glass required to shield more energetic photons is higher due to a decrease in the interaction coefficients of high-energy photons.

In Fig. 4, the attenuation of GZr8Al8 is placed in contrast to a wide variety of shielding materials based on the values λ for wide energy range. The compared materials include Schott glasses[57–59], other glasses (PBZH3[60], PBCN-M4[61], S8[62], ZBP4[63], and BSNW4[64], different types of concrete compositions (ordinary (OC), hematite-serpentine (HS), ilmenite-limonite (IL), basalt-magnetite (BM), ilmenite (IN), steel-scrap (SS), and steel-magnetite (SM) concretes)[65], and other composite materials including polymers (P2)[66], guanine [67], rocks (VR3)[68], and alloys (FBCSP1)[69]. The mean free path of GZr8Al8 appears lower than those of RS253 and RS253G18 but higher than those of RS253G19 and RS360 at three distinct gamma energies, as seen in

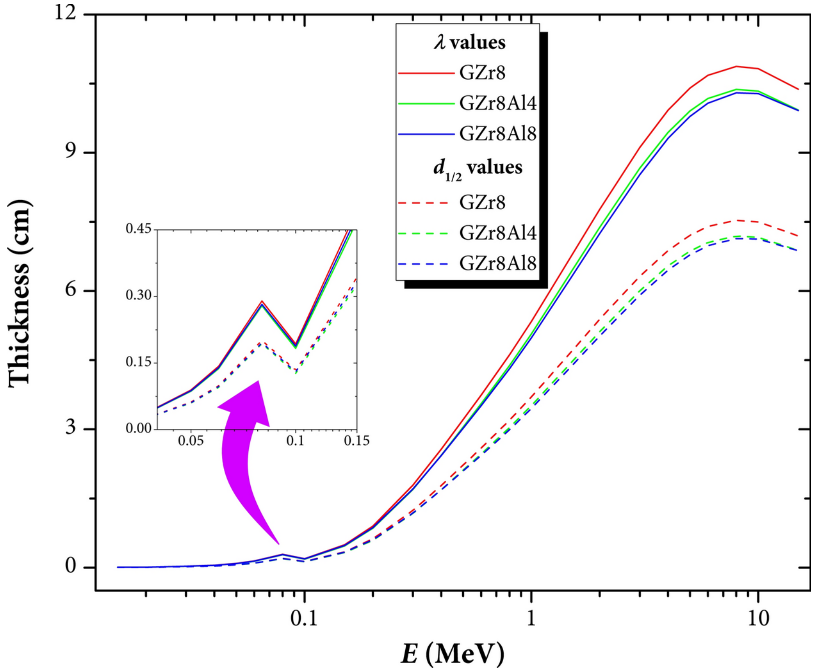

Fig. 3. Mean free path (λ, solid line) and half value layer ($d_{1/2}$, dash line) variations with respect to f photon energy in the prepared glasses.

Fig. 4a. This affirms the superior gamma absorption ability of GZr8Al8 compared to RS253 and RS253G18. The fact that GZr8Al8 is Pb-free adds to the comparative advantage of the glass relative to these two commercial glasses. In addition, GZr8Al8 can absorb photons better than all five different shielding glasses compared in Fig. 4b for most of the 15 keV–15 MeV energy spectrum. In Fig. 4c, the photon absorption prowess of GZr8Al8 relative to the light and dense concrete samples is superior at energies below 100 keV. Above this energy, only SS and SM could outshine GZr8Al8 in attenuating photons. Finally, in Fig. 4d, GZr8Al8 showed better gamma shielding competence compared to other composite materials, except FBCSP1. The mean free path of GZr8Al8 is comparable to that of FBCSP1 at energies below 500 keV and lower for the rest of the energy spectrum. From Fig. 4, it is clear that GZr8Al8 can displace many existing shielding materials including glasses, concrete, and rocks. The mechanical strength of the glass and Pb-free composition are other attractive features of GZr8Al8 that give it an edge over many existing gamma shielding materials. GZr8Al8 is an attractive shielding material from toxicity and mechanical strength perspectives. The glass is thus recommended for shielding of laboratory sources and other places where hard material is required.

The Z_{eff} and N_{eff} of a composite material are quick parameters for identifying equivalent materials for shielding applications. When it comes to photon interactions, Z_{eff} is to a chemical compound or mixture what Z is to pure atoms, while N_{eff} is a measure of the average Z/A of a composite medium. The values of Z_{eff} and N_{eff} for different energies are plotted for GZr8, GZr8Al4, and GZr8Al8 in Fig. 5. Both quantities vary similarly with E. The values of Z_{eff} and N_{eff} vary from 14.65–55.13 and 2.92×10^{23}–10.99 electrons/g for GZr8, 14.41–55.74 and 2.92×10^{23}–11.17×10^{23} electrons/g for GZr8Al4, and 14.10–55.01 and 2.93×10^{23}–11.18×10^{23} electrons/g for GZr8Al8. The energy variations and the order of Z_{eff} is predicted by the main interaction process at a particular energy, as predicted by Eqs. (3)-(5). The order of Z_{eff} and N_{eff} vary inversely from one another due to the decrease in the average Z/A value with respect to Z.

For dosimetry purposes, $\frac{\mu_{en}}{\rho}$, Γ, and D_r are important quantities for a medium. The mass attenuation coefficient and $\frac{\mu_{en}}{\rho}$ are similar, while the former gives a measure of total photon interaction in a medium, the latter quantifies the amount of photon energy absorbed from the interactions. Both quantities are directly proportional and the ratio of ${}^{\mu/\rho}/_{\mu_{en}/\rho}$ gives the ratio of the incident photon energy to that absorbed in a medium. This explains why the energy variations of $\frac{\mu_{en}}{\rho}$ shown in Fig. 6a is similar to that of μ/ρ. The explanation describing the energy variation of μ/ρ suffices for $\frac{\mu_{en}}{\rho}$. The maximum $\frac{\mu_{en}}{\rho}$ values of 32.80 cm^2/g, 32.6818 cm^2/g, and 31.22098 cm^2/g for GZr8, GZr8Al4, and GZr8Al8 was obtained at 15 keV.

The absorbed dose due to a radioactive (gamma) source positioned one-meter away from an absorber is proportional to the specific constant (Γ). Figure 6b plots Γ against energy for GZr8, GZr8Al4, and GZr8Al8. The dose absorbed in a medium is directly proportional to $\frac{\mu_{en}}{\rho}$, E, distance from the source, absorber thickness, and the photon source strength[70]. The energy response of Γ is dictated by photon energy and $\frac{\mu_{en}}{\rho}$. Therefore, the energy response is similar to that of $\frac{\mu_{en}}{\rho}$ for energy below 1 MeV. The high energy and pair production absorption process is responsible for the increase in the Γ-values of the glasses. Comparatively, AlON-deficient glasses had higher Γ at energies below 1 MeV due to photoelectric absorption of photons at absorption edges of low-Z atoms. Above this energy, the differences in the glasses do not significantly results in different values of Γ.

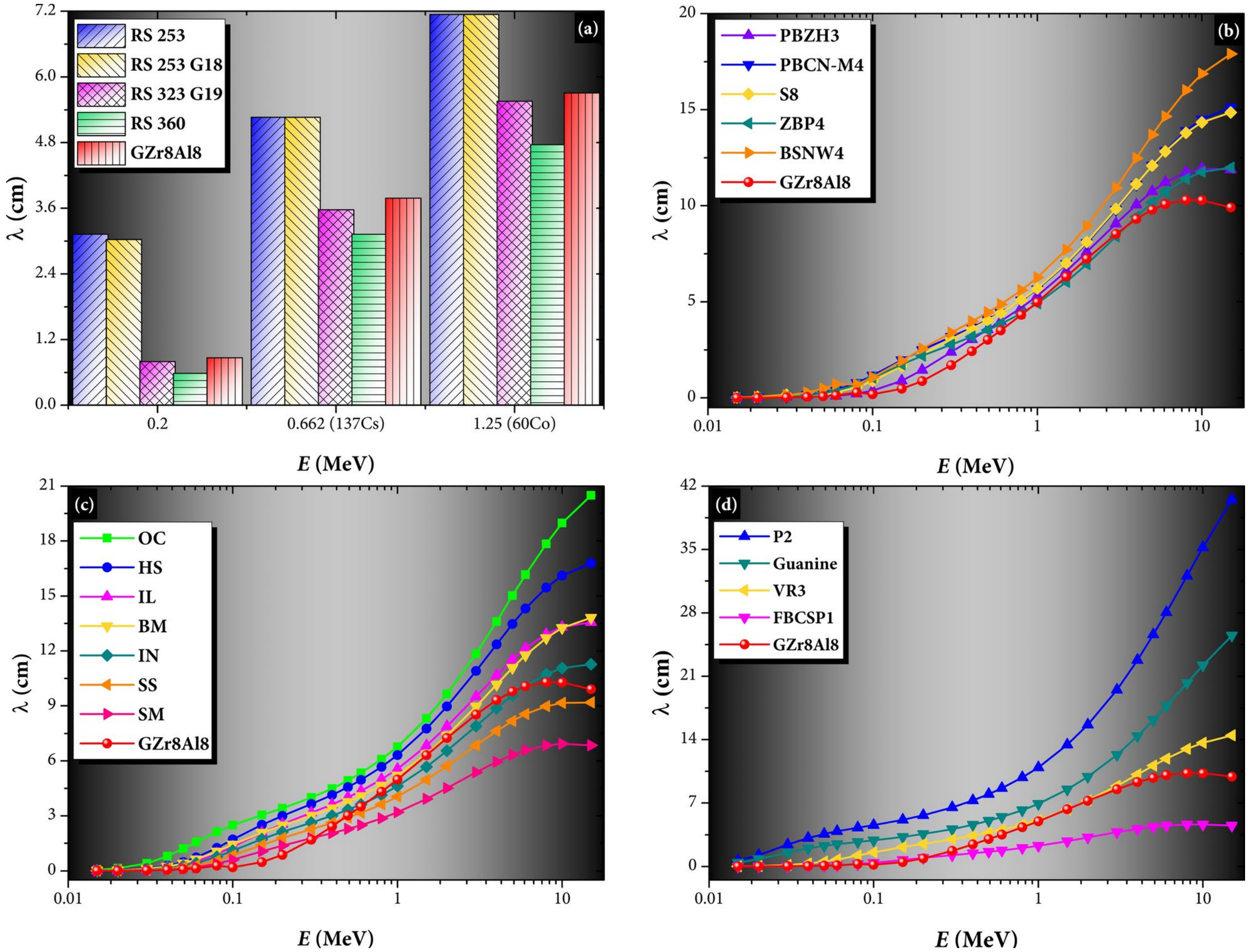

Fig. 4. Comparison of mean free path (λ) parameter of the prepared GZr8Al8 glass with those in (**a**) commercial SCHOTT's radiation shielding glasses[57–59], (**b**) some glass systems[60–64], (**c**) standard shielding concretes[65], and (**d**) polymer-composite materials[66–69].

The absorbed doses in different thicknesses of the glasses are displayed in Fig. 7.

The figure shows plots of D_r against energy for glass thicknesses of 1 mm, 5 mm, 10 mm, and 15 mm. Due to geometric and exponential attenuations, the photon dose rate slows down with the thickness of the glass and vary directly as Γ. The highest dose rates values were obtained at 15 keV for GZr8, with value of 324 MR/hfor 1 mm glass thicknesses. For GZr8Al4, the value is 322 MR/h, while the corresponding value for GZr8Al8is 324 MR/h, respectively. The differences between the dose rates are very thin, especially at high energies. At equal thickness and the same photon energy, AlON-deficient glass has higher D_r due to lower $\frac{\mu_{en}}{\rho}$.

Photons suffer two fates after interaction with matter: they are scattered or absorbed. Scattering compromises shielding; hence, a good shield should completely absorb photons within the energy spectrum of the application. The scattering of photons leads to photon-build-up within the interacting medium. The buildup affects different radiation quantities in different ways; therefore, buildup factors are named depending on the interaction quantity of interest. The exposure and energy absorption (EBF and EABF) of GZr8, GZr8Al4, and GZr8Al8 were computed and plotted for different gamma radiation path within 40 mfp in Fig. 8 and Fig. 9. The buildup factors increase with the thickness due to multiple scatterings in thicker glasses. The buildup factors (BUFs) are higher at the energy region where incoherent scattering dominates the interaction processes. In addition, increasing BUFs were observed at the end of the energy spectrum due to scattering of low-energy photons released due to the annihilation of positron–electron pairs. Unusually high BUFs were also recorded at 30 keV for all the glasses. The intensity of this spike, however, reduces as AlON content increases. The reduction in the BUF spike can be attributed to the scattering of photons released during the de-excitation of Ba atoms, whose absorption edge is around 37 keV. This shows that the application of a shield at an energy close to the absorption edge of its constituent atom may not be efficient; a material is transparent to its fluorescence. The introduction of AlON, however, quenched the BUFs. The doping of AlON into the matrix of studied glasses quenches BUFs and enhances photon shielding ability of the GZr8 glass system (Fig. 9).

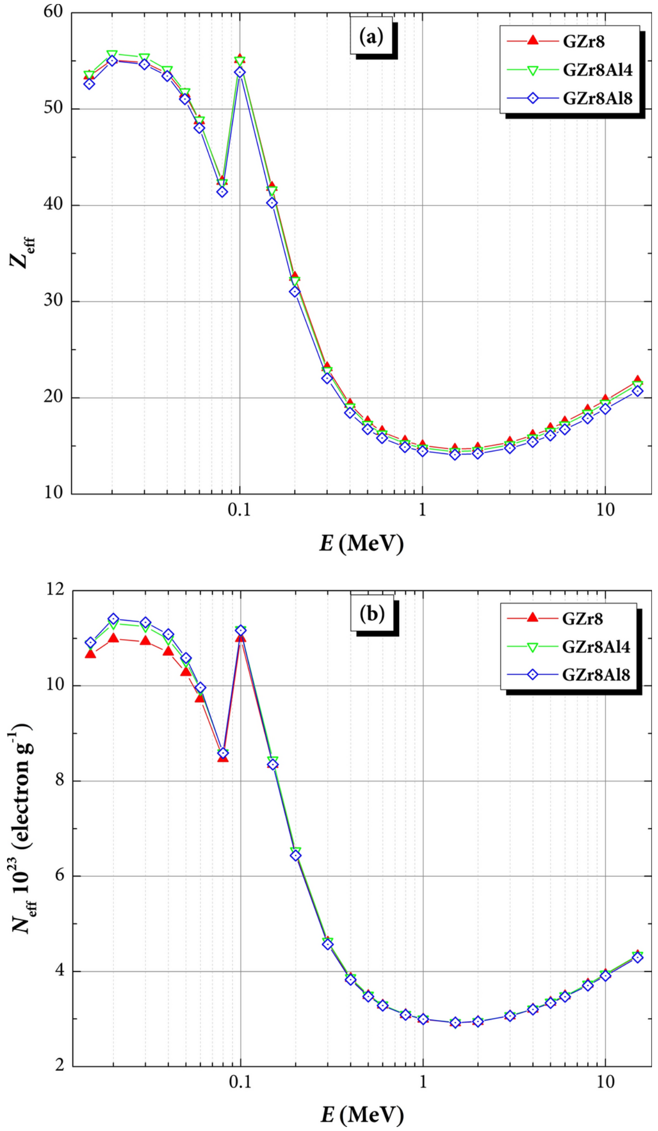

Fig. 5. (**a**) Effective atomic number and (**b**) effective electron density of the prepared glasses with different photon energies.

Conclusion

The melt-and-quench process was used to fabricate the Zr-based (Na_2O–Bi_2O_3–SiO_2–BaO–Fe_2O_3–ZrO_2) glass, which was homogeneously mixed with AlON powder in varying quantities (0, 4, and 8% by weight). The measured density of the glasses increased from 2.90 to 3.11 g/cm3, and the hardness increased from 4.89 to 6.33 GPa as the AlON mass proportion increased from 0 to 8%. AlON could thus increase the resilience of the glasses against mechanical failure and deformation, making them useful in high strength applications. The introduction of AlON increased the effective Z and atomic density of the glasses. $d_{1/2}$. The values Z_{eff} and N_{eff} vary from 14.65–55.13 and 2.92×10^{23}–10.99 electrons/g for GZr8, 14.41–55.74 and 2.92×10^{23}–11.17×10^{23} electrons/g for GZr8Al4, and 14.10–55.01 and 2.93×10^{23}–11.18×10^{23} electrons/g for GZr8Al8. The order Z_{eff} and N_{eff} vary inversely to one another due to the decrease in the average Z/A value with respect to Z. The maximum $\frac{\mu_{en}}{\rho}$ values of 32.80 cm^2/g, 32.6818 cm^2/g, and 31.22098 cm^2/g for GZr8, GZr8Al4, and GZr8Al8 were obtained at 15 keV. AlON-deficient glasses had higher Γ at energies below 1 MeV due to the photoelectric absorption of photons at the absorption edges of low-Z atoms. AlON reduced photon transmission through the glasses and prevent photon build up in them. GZr8Al8 good potential to displace many existing shielding materials, including commercial and recently recommended shielding glasses, shielding concrete samples, and rocks, in shielding applications. The AlON-rich glass can be used for radiation source shielding in medicine, laboratory, and places where tough glasses are required. The use of AlON to increase density, mechanical strength, and gamma-radiation interaction properties of other glass and ceramic materials could be used to increase their durability in radiation environment. The impact of radiation on the general properties of the glasses and ceramics could however be studied to highlight their stability in radiation environments.

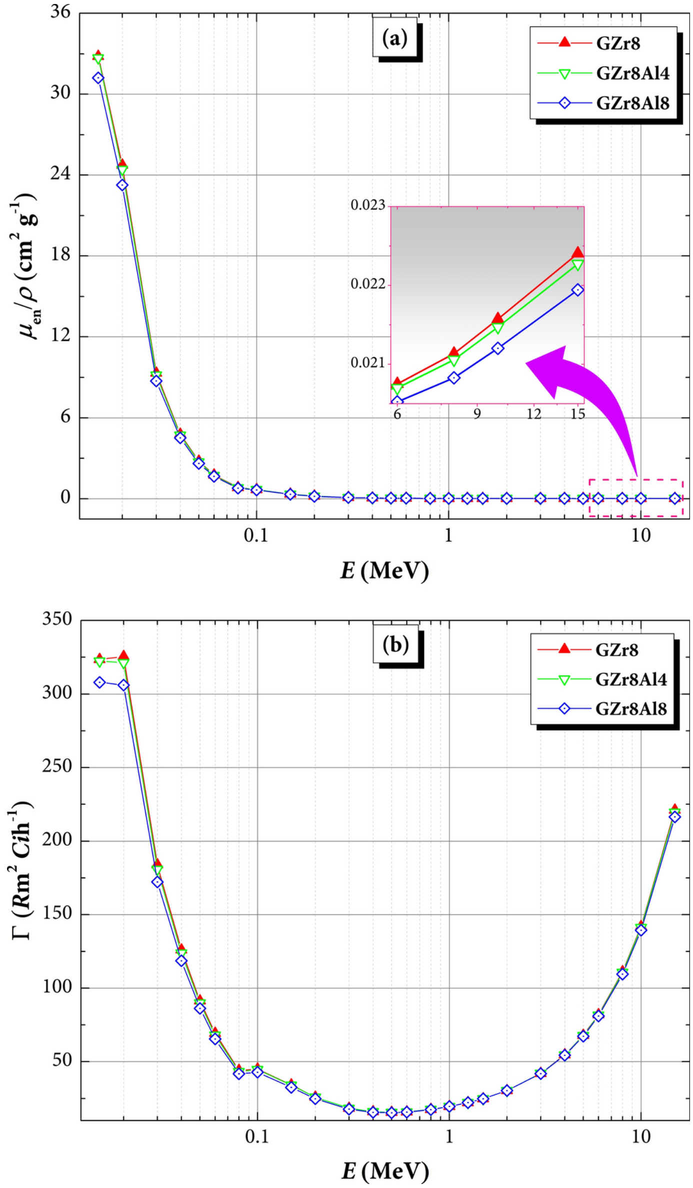

Fig. 6. (**a**) Mass energy-absorption coefficient and (**b**) specific gamma ray constant of the prepared glasses with different photon energies.

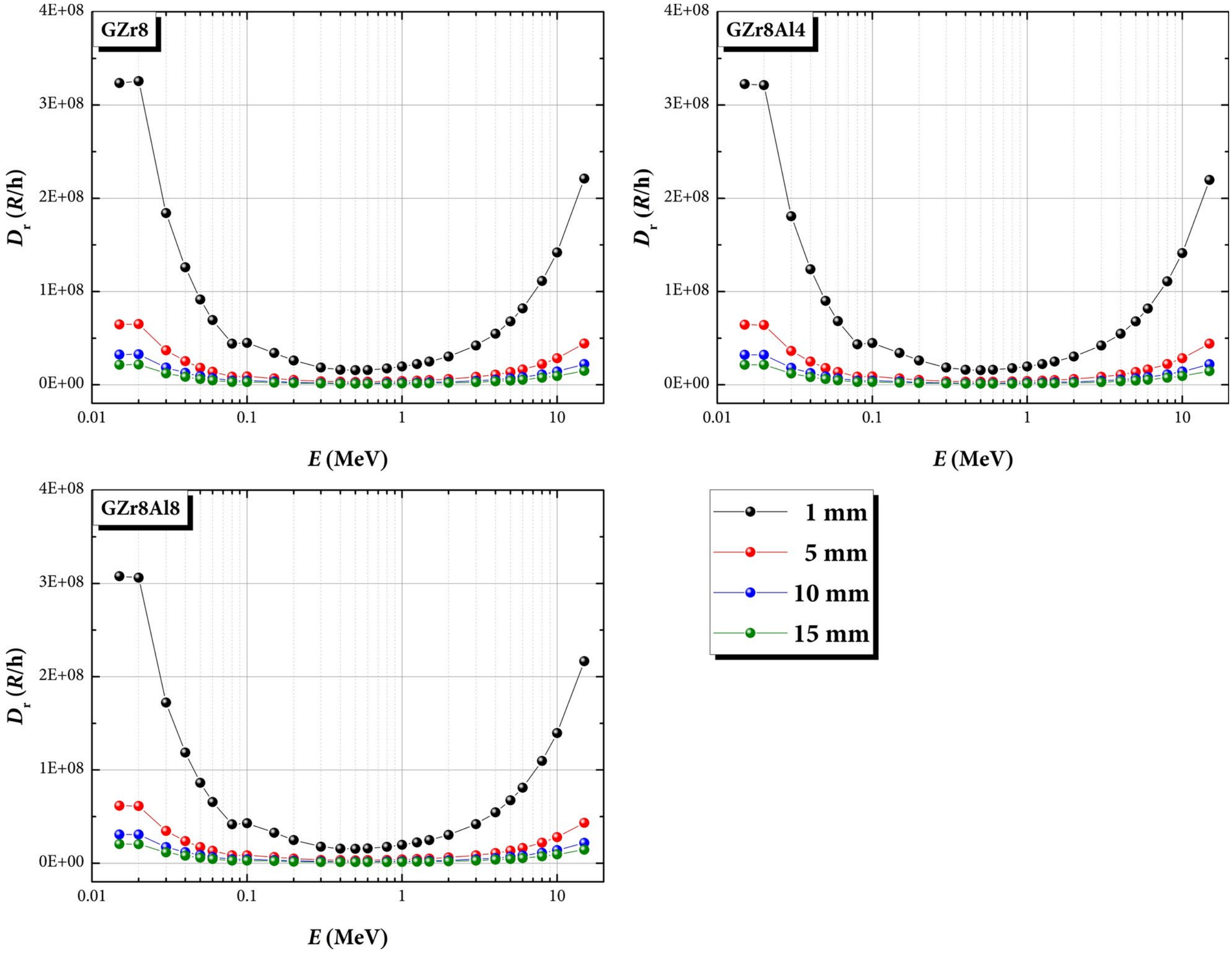

Fig. 7. Gamma dose rate (D_r) at different energies and glass thicknesses.

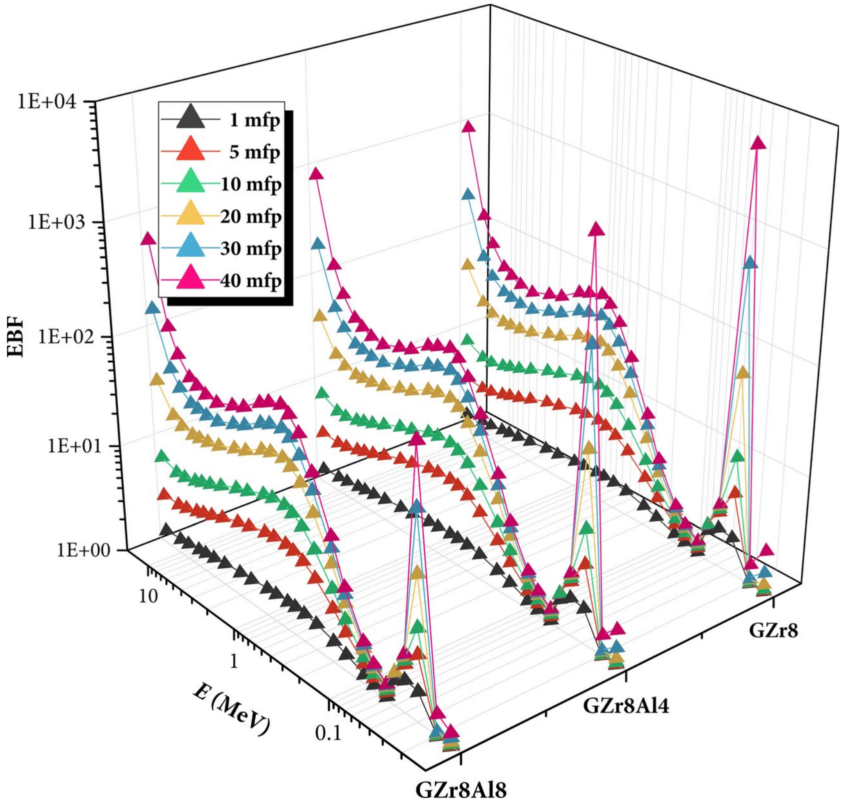

Fig. 8. Exposure buildup factor (EBF) with respect to the concentration of Bi and a function of photon energy in the prepared glasses.

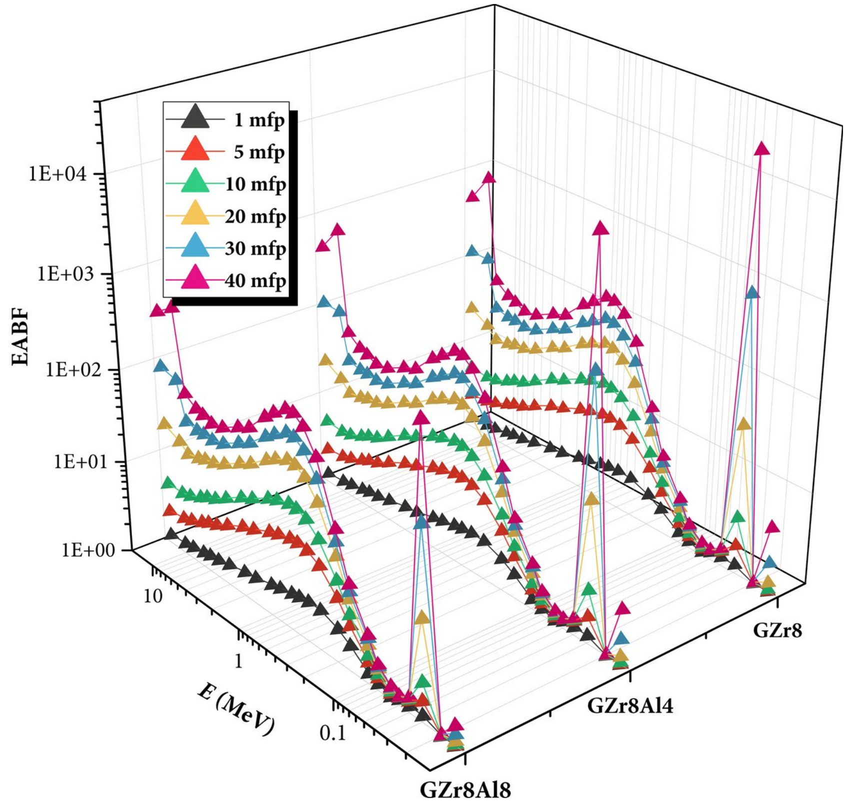

Fig. 9. Energy absorption buildup factor (EABF) with respect to the concentration of Bi and a function of photon energy in the prepared glasses.

Data availability

The authors declare that the data supporting the findings of this study are available within the paper.

Received: 27 May 2024; Accepted: 17 February 2025
Published online: 24 February 2025

References

1. Gomes, A. D., de Oliveira, A. A., Houmard, M. & Nunes, E. H. Gamma sterilization of collagen/hydroxyapatite composites: Validation and radiation effects. *Appl. Radiat. Isot.* **174**, 109758 (2021).
2. Finnberg, N., Wambi, C., Ware, J. H. & Kennedy, A. R. Gamma-radiation (GR) triggers a unique gene expression profile associated with cell death compared to proton radiation (PR) in mice in vivo. *Cancer Biol. Ther.* **7**(12), 2023–2033 (2008).
3. Ogundare, F. O., Olarinoye, I. O. & Obed, R. I. Estimation of patients' organ doses and conceptus doses from selected X-ray examinations in two Nigeria X-ray centres. *Radiat. Prot. Dosimetry* **132**(4), 395–402 (2008).
4. Kaboré, B. A. et al. X-rays are as effective as gamma-rays for the sterilization of Glossina palpalis gambiensis Vanderplank, 1911 (Diptera: Glossinidae) for use in the sterile insect technique. *Sci. Rep.* **13**(1), 17633 (2023).
5. Silindir, M. & Özer, A. Y. Sterilization methods and the comparison of E-beam sterilization with gamma radiation sterilization. *Fabad J. Pharm. Sci.* **34**(1), 43 (2009).
6. Olarinoye, I. O. & Ogundare, F. O. Optical and microstructural properties of neutron irradiated RF-sputtered amorphous alumina thin films. *Optik* **134**, 66–77 (2017).
7. Ogundare, F. O. & Olarinoye, I. O. He+ induced changes in the surface structure and optical properties of RF-sputtered amorphous alumina thin films. *J. Non-Cryst. Solids* **432**, 292–299 (2016).
8. Naikwadi, A. T., Sharma, B. K., Bhatt, K. D. & Mahanwar, P. A. Gamma radiation processed polymeric materials for high performance applications: A review. *Front. Chem.* **10**, 837111 (2022).
9. Bakri, A., Mehta, K., Lance, D. R., Dyck, V. A., Hendrichs, J. & Robinson, A. S. Sterilizing insects with ionizing radiation.in *Sterile Insect Technique: Principles and Practice in Area-Wide Integrated Pest Management*, 355–398 (2021).
10. Abdelnour-Esquivel, A., Perez, J., Rojas, M., Vargas, W. & Gatica-Arias, A. Use of gamma radiation to induce mutations in rice (Oryza sativa L.) and the selection of lines with tolerance to salinity and drought. *In Vitro Cell. Dev. Biol.-Plant* **56**, 88–97 (2020).
11. Shahboub, A., El Damrawi, G. & Saleh, A. A new focus on the role of iron oxide in enhancing the structure and shielding properties of Ag2O–P2O5 glasses. *Eur. Phys. J. Plus* **136**(9), 947 (2021).
12. Shahboub, A., Saleh, A., Hassan, A. K. & Damrawi, G. E. EPR studies and radiation shielding properties of silver aluminum phosphate glasses. *Appl. Phys. A* **129**(6), 410 (2023).
13. Saleh, A., Elshazly, R. & Abd Elghany, H. The impact of CdO on the radiation shielding properties of zinc–sodium–phosphate glass containing barium. *Arab J. Nucl. Sci. Appl.* **55**(1), 116–126 (2022).
14. Saleh, A., El-Feky, M. G., Hafiz, M. S. & Kawady, N. A. Experimental and theoretical investigation on physical, structure and protection features of TeO_2–B_2O_3 glass doped with PbO in terms of gamma, neutron, proton and alpha particles. *Radiat. Phys. Chem.* **202**, 110586 (2023).

15. Saleh, A., Mansour, F. E. & Abdelhakim, N. A. An appropriate balance of mechanical and ionized radiation shielding performance across some tin binary alloys: A comparative investigation. *Radiat. Phys. Chem.* **221**, 111726 (2024).
16. Saleh, A., Almohiy, H., Shalaby, R. M. & Saad, M. Comprehensive investigation on physical, structural, mechanical and nuclear shielding features against X/gamma-rays, neutron, proton and alpha particles of various binary alloys. *Radiat. Phys. Chem.* **216**, 111443 (2024).
17. Adib, M., Habib, N., Bashter, I. & Saleh, A. Neutron transmission through pyrolytic graphite crystal II. *Ann. Nucl. Energy* **38**(4), 802–807 (2011).
18. Adib, M. et al. Neutron characteristics of single-crystal magnesium fluoride. *Ann. Nucl. Energy* **60**, 163–171 (2013).
19. Abd-Elkader, O. H. et al. Rapid fabrication, magnetic, and radiation shielding characteristics of $NiFe_2O_4$ nanoparticles. *Opt. Mater. Exp.* **14**(5), 1170–1185 (2024).
20. Ezra, N. S. et al. Synthesis, and impact of GaN deposition on the physical, optical, and structural properties of Nd3+-doped Na_2O borate glasses prepared with soda lime (SLS) glass as a silica source. *Opt. Mater.* **155**, 115907 (2024).
21. Khazaalah, T. H. et al. The effect of wo3-doped soda lime silica sls waste glass to develop lead-free glass as a shielding material against radiation. *Sustainability* **14**(4), 2413 (2022).
22. Ezra, N. S. et al. Synthesis and Effect of MgSO4 co-doping on the optical, IR, and Raman Spectroscopic Studies of Eu3+-doped alkaline silica borate glasses produced with sls glass as a silica source. *Silicon* **16**(17), 6085–6097 (2024).
23. Ezra, N. S. et al. Review of recycled soda–lime–silicate (SLS) glasses for dosimetric applications. *Radiat. Phys. Chem.* https://doi.org/10.1016/j.radphyschem.2024.112085 (2024).
24. Khazaalah, T. H., Mustafa, I. S. & Sayyed, M. I. Radiation parameterizations and optical characterizations for glass shielding composed of SLS waste glass and lead-free materials. *Nucl. Eng. Technol.* **54**(12), 4708–4714 (2022).
25. Naeem, H. S. et al. High sensitivity transparent glass ceramic systems development based on $MgSO_4$: Dy_2O_3–B_2O_3 and $MgSO_4$: Dy_2O_3–B_2O_3: ZnO: An investigation of FT-IR and thermal properties for thermoluminescence dosimeter applications. *Opt. Mater.* **156**, 116003 (2024).
26. Khazaalah, T. H. et al. Development of novel transparent radiation shielding glasses by BaO doping in waste soda lime silica (SLS) glass. *Sustainability* **14**(2), 937 (2022).
27. Olarinoye, I. O. et al. The effects of La2O3 addition on mechanical and nuclear shielding properties for zinc borate glasses using Monte Carlo simulation. *Ceram. Int.* **46**(18), 29191–29198 (2020).
28. Tamam, N. et al. Radiation attenuation of boro-tellurite glasses for efficient shielding applications. *Appl. Radiat. Isotopes* **203**, 111080 (2024).
29. Sailaja, P. et al. Effect of Eu3+ ions concentration on visible red luminescence and radiative shielding properties of SrO–Al_2O_3–$BaCl_2$–B_2O_3–TeO_2 glasses. *Radiat. Phys. Chem.* **216**, 111467 (2024).
30. Alomayrah, N., Alrowaili, Z. A., Eke, C., Olarinoye, I. O. & Al-Buriahi, M. S. Radiation shielding efficacy of zinc-lithium-borate glasses: Theoretical study. *J. Radiat. Res. Appl. Sci.* **17**(1), 100837 (2024).
31. Solak, B. B. et al. Exploring the radiation shielding properties of B_2O_3–PbO–TeO_2–CeO_2–WO_3 glasses: A comprehensive study on structural, mechanical, gamma, and neutron attenuation characteristics. *Mater. Chem. Phys.* **312**, 128672 (2024).
32. Katubi, K. M. et al. Radiation Shielding efficiency of lead-tungsten-boron glasses with Sb, Al, and Bi against gamma, neutron and charge particles. *Appl. Radiat. Isotopes* **204**, 111139 (2024).
33. Babeer, A. M., Sayyed, M. I., Amin, H. Y., Mahmoud, A. E. R. & Sadeq, M. S. Composition impacts of La_2O_3 on the structure and radiation shielding parameters of NiO–BaO–B_2O_3 glasses. *Opt. Mater.* **147**, 114622 (2024).
34. Wondraczek, L. et al. Advancing the mechanical performance of glasses: perspectives and challenges. *Adv. Mater.* **34**(14), 2109029 (2022).
35. Ha, M. H., Choi, J. K., Park, B. M. & Han, K. Y. Highly flexible cover window using ultra-thin glass for foldable displays. *J. Mech. Sci. Technol.* **35**, 661–668 (2021).
36. Garner, S. M., Li, X. & Huang, M. H. Introduction to flexible glass substrates. *Flex. Glass: Enabling Thin Lightweight Flex. Electron.* https://doi.org/10.1002/9781118946404 (2017).
37. Al-Buriahi, M. S., Alsaiari, N. S., Baskin, M. U. & Olarinoye, I. O. Recent progress in the radiation shielding performance of common glass systems: The roles of different class of modifiers. *J. Radiat. Res. Appl. Sci.* **18**(1), 101264 (2025).
38. Al-Buriahi, M. S., Kurtulus, R., Eke, C., Alomairy, S. & Olarinoye, I. O. An insight into advanced glass systems for radiation shielding applications: A review on different modifiers and heavy metal oxides-based glasses. *Heliyon* **10**(22), e40249 (2024).
39. Liu, X. J. et al. Hard transparent AlON ceramic for visible/IR windows. *Int. J. Refract. Metals Hard Mater.* **39**, 38–43 (2013).
40. Liu, Q. et al. Highly transparent AlON ceramics sintered from powder synthesized by carbothermal reduction nitridation. *Ceram. Int.* **42**(7), 8290–8295 (2016).
41. Berger, M. J. NIST XCOM: photon cross sections database (2010). http://www.nist.gov/pml/data/xcom/index.cfm.
42. Ballarini, F. et al. The FLUKA code: An overview. *J. Phys.: Conf. Ser.* **41**(1), 15 (2006).
43. Böhlen, T. T. et al. The FLUKA code: Developments and challenges for high energy and medical applications. *Nucl. Data Sheets* **120**, 211–214 (2014).
44. Battistoni, G. et al. Applications of FLUKA Monte Carlo code for nuclear and accelerator physics. *Nucl. Instrum. Methods Phys. Res. Sect. B: Beam Interact. Mater. Atoms* **269**(24), 2850–2856 (2011).
45. Katubi, K. M., Alrowaili, Z. A., Olarinoye, I. O. & Al-Buriahi, M. S. Optical properties and radiation protection applications of B_2O_3: Na_2O: PbO: Tb_2O_3: Bi_2O_3 glass system. *Opt. Quant. Electron.* **56**(4), 625 (2024).
46. Samdani, M. et al. Gamma shielding performance of B_2O_3/BaO-based glassy system: Synthesis and simulation study. *Radiat. Phys. Chem.* **214**, 111301 (2024).
47. Rammah, Y. S. et al. Responsibility of Bi_2O_3 content in photon, alpha, proton, fast and thermal neutron shielding capacity and elastic moduli of ZnO/B_2O_3/Bi_2O_3 glasses. *J. Inorgan. Organometall. Polym. Mater.* **31**, 3505–3524 (2021).
48. Yorgun, N. Y., Kavaz, E., Tekin, H. O., Sayyed, M. I. & Özdemir, Ö. F. Borax effect on gamma and neutron shielding features of lithium borate glasses: An experimental and Monte Carlo studies. *Mater. Res. Exp.* **6**(11), 115217 (2019).
49. Oto, B., Çakar, N., Kavaz, E. & Madak, Z. An experimental study on gamma radiation attenuation effectiveness of magnetite and serpentine doped ceramics. *Progress Nucl. Energy* **169**, 105079 (2024).
50. Rammah, Y. S., Olarinoye, I. O., El-Agawany, F. I. & El-Adawy, A. The f-factor, neutron, gamma radiation and proton shielding competences of glasses with Pb or Pb/Bi heavy elements for nuclear protection applications. *Ceram. Int.* **46**(17), 27163–27174 (2020).
51. Prakash, A. H. D. et al. Synthesis and characterization of B_2O_3–Bi_2O_3–SrO–Al_2O_3–PbO–Dy_2O_3 glass system: The role of Bi2O3/Dy2O3 on the optical, structural, and radiation absorption parameters. *Mater. Res. Bull.* **155**, 111952 (2022).
52. Naderi, D., Ahmadi, M. & Zanganeh, V. Effect of rare-earth oxide (Eu2O3) on the physical, mechanical, acoustic and radiation shielding properties of the CaO-Gd_2O_3–SiO_2–B_2O_3 glasses. *Appl. Radiat. Isotopes* **208**, 111309 (2024).
53. Ahmadi, M., Vahid, Z. & Darush, N. Investigated mechanical, physical parameters and Gamma-Neutron radiation shielding of the rare earth (Er_2O_3/CeO_2) doped barium borate glass: Role of the melting time and temperature. *Radiat. Phys. Chem.* **217**, 111450 (2024).
54. Karami, H., Zanganeh, V. & Ahmadi, M. Effect of B_2O_3/Bi_2O_3 on radiation shielding parameters of mobile phone waste glasses (2024).
55. Asri, M., Ahmadi, M. & Zanganeh, V. CuO-doping effect on the optical properties (linear/linear terrace) and mechanical and acoustic features of lead borate glasses. *J. Mater. Sci.: Mater. Electron.* **34**(26), 1820 (2023).

56. Asri, M., Ahmadi, M. & Zanganeh, V. Study of optical properties and comprehensive shielding behaviors for neutron and gamma-ray of $60Bi_2O_3$-(40–x) B_2O_3-xBaO glass system. *Res. Phys.* **52**, 106824 (2023).
57. Speid, B. Radiation-shielding glasses providing safety against electrical discharge and being resistant to discoloration. Google Patents (1991). https://patents.google.com/patent/US5073524A/en Accessed 30 Oct 2021.
58. https://www.schott.com/en-ca/products/radiation-shielding-glasses/product-variants?tab=rs-glass-series. Accessed 30 Nov 2023.
59. Kaur, P., Singh, K. J., Thakur, S., Singh, P. & Bajwa, B. S. Investigation of bismuth borate glass system modified with barium for structural and gamma-ray shielding properties. *Spectrochim. Acta A Mol. Biomol. Spectrosc.* **206**, 367–377 (2019).
60. Alharshan, G. A., Alrowaili, Z. A., Olarinoye, I. O. & Al-Buriahi, M. S. Holmium (III) oxide and its significant effects on the radiation shielding performance of P2O5+ B2O3+ ZnSO4 optical glasses. *Optik* **261**, 169188 (2022).
61. Alharshan, G. A. et al. Optical borophosphate glass system with excellent properties for radiation shielding applications. *Optik* **266**, 169568 (2022).
62. Singh, J. et al. Optical and radiation shielding features for some phospho-silicate glasses. *Optik* **261**, 169140 (2022).
63. Alothman, M. A. et al. Elastic properties and radiation shielding ability of $ZnO–P_2O_5/B_2O_3$ glass system. *J. Mater. Sci.: Mater. Electron.* **32**(14), 19203–19217 (2021).
64. Al-Buriahi, M. S., Taha, T. A., Alothman, M. A., Donya, H. & Olarinoye, I. O. Influence of WO3 incorporation on synthesis, optical, elastic and radiation shielding properties of borosilicate glass system. *Eur. Phys. J. Plus* **136**(7), 779 (2021).
65. Bashter, I. I. Calculation of radiation attenuation coefficients for shielding concretes. *Ann. Nucl. Energy* **24**(17), 1389–1401 (1997).
66. Al-Buriahi, M. S. et al. Radiation attenuation properties of some commercial polymers for advanced shielding applications at low energies. *Polym. Adv. Technol.* **32**(6), 2386–2396 (2021).
67. Al-Buriahi, M. S., Sriwunkum, C. & Boukhris, I. X-and gamma-rays attenuation properties of DNA nucleobases by using FLUKA simulation code. *Eur. Phys. J. Plus* **136**(7), 776 (2021).
68. Saeed, A., Alomairy, S., Sriwunkum, C. & Al-Buriahi, M. S. Neutron and charged particle attenuation properties of volcanic rocks. *Radiat. Phys. Chem.* **184**, 109454 (2021).
69. Alshahrani, B. et al. Amorphous alloys with high Fe content for radiation shielding applications. *Radiat. Phys. Chem.* **183**, 109386 (2021).
70. Alzahrani, J. S. et al. Synthesis, photoluminescence and gamma attenuation properties of europium-doped borate glasses. *Opt. Mater.* **144**, 114363 (2023).

Acknowledgements
The authors express their gratitude to Princess Nourah bint Abdulrahman University Researchers Supporting Project number (PNURSP2025R48), Princess Nourah bint Abdulrahman University, Riyadh, Saudi Arabia. Moreover, the authors extend their appreciation to the Deanship of Research and Graduate Studies at King Khalid University, Saudi Arabia for funding this work through Large Groups Project under grant number R.G.P2/76/46.

Author contributions
Jamila S. Alzahrani, Z.A. Alrowaili, I.O. Olarinoye, Chahkrit Sriwunkum, Imen Kebaili, and M.S. Al-Buriahi wrote the main manuscript text and prepared figures. All authors reviewed the manuscript.

Declarations

Competing interests
The authors declare no competing interests.

Additional information
Correspondence and requests for materials should be addressed to J.S.A.

Reprints and permissions information is available at www.nature.com/reprints.

Publisher's note Springer Nature remains neutral with regard to jurisdictional claims in published maps and institutional affiliations.